

Comparative chemistry of diffuse clouds

V. Ammonia and formaldehyde

H. S. Liszt¹, R. Lucas², and J. Pety^{2,3}

¹ National Radio Astronomy Observatory, 520 Edgemont Road, Charlottesville, VA, 22903-2475, USA
e-mail: hliszt@nrao.edu

² Institut de Radioastronomie Millimétrique, 300 Rue de la Piscine, 38406 Saint Martin d'Hères, France

³ Obs. de Paris, 61 av. de l'Observatoire, 75014, Paris, France

Accepted 15 August 2005 / Accepted 3 November 2005

ABSTRACT

Using the VLA and NRAO 140' telescopes we observed the $\lambda 1.3$ cm (1, 1) and (2, 2) lines of NH_3 in absorption and emission toward the compact extragalactic continuum sources NRAO150 (B0355+508) and 3C 111 (B0415+379). These sources are occulted by some seven local diffuse and translucent clouds showing molecular absorption in OH, CO, HCO^+ and C_2H : for the four features having NH_3 absorption, we find rotational excitation temperatures 18–24 K, suggesting kinetic temperatures of at least 25–30 K.

The abundance ratio $N(\text{NH}_3)/N(\text{HCO}^+)$ is comparable to values quoted for the cyanopolyne peak in TMC-1 (i.e., 2.5) in three of four cases where NH_3 was seen. For clouds with higher column density $N(\text{HCO}^+) \gtrsim 10^{12} \text{ cm}^{-2}$, the NH_3 column density $N(\text{NH}_3)$ is well correlated only with $N(\text{CS})$ ($\langle N(\text{NH}_3)/N(\text{CS}) \rangle \approx 1.0$) and $N(\text{H}_2\text{CO})$ ($\langle N(\text{NH}_3)/N(\text{H}_2\text{CO}) \rangle \approx 0.4$). $N(\text{H}_2\text{CO})$ is well correlated with $N(\text{NH}_3)$ and $N(\text{CS})$ ($\langle N(\text{H}_2\text{CO})/N(\text{CS}) \rangle \approx 2.3$) and the H_2CO abundance relative to other species is like TMC-1, with ($\langle N(\text{H}_2\text{CO})/N(\text{HCO}^+) \rangle \approx 2.3$).

Key words. ISM: molecules

1. Introduction

Ammonia and formaldehyde are hardly thought of as common molecules in diffuse clouds but Nash (1990) detected both in absorption toward the compact extragalactic radiocontinuum source B0355+508 (NRAO150), against which Cox et al. (1988) had earlier seen C_3H_2 in absorption “in the diffuse interstellar medium”. Unfortunately there is no evidence in Nash’s work that she was aware of the C_3H_2 detection – her observations were actually taken prior to 1988 – and she characterized the absorption features in question as arising in “molecular clouds.” In retrospect, it now seems clear that many of the H_2CO features seen in the galactic plane against galactic HII regions arise in diffuse clouds and it is clear that H_2CO lines, if not the most ubiquitous spectral features, are seen along sight-lines where the gas cannot by any means be characterized as very dark or dense (Liszt & Lucas 1995; Moore & Marscher 1995).

Ammonia and formaldehyde have in common the fact that both have been subject to considerable uncertainty as to their formation mechanisms in dense dark gas, being at times understood as only capable of formation on grain surfaces. It is now recognized that NH_3 may be produced in the gas phase in dark clouds via the reaction of N^+ and H_2 (Le Bourlot 1991) or N and H_3^+ (Scott et al. 1997) but its origin in more diffuse gas is obscure. Federman & Allen (1991) argued that H_2CO could be

seen at extinctions of $A_V = 1$ mag at the edges of dark clouds, having formed on grains and then diffused or convected out of the protected inner regions. However, maps of extinction toward lines of sight in which H_2CO is seen at $A_V \leq 1$ mag do not generally reveal the presence of nearby dark clouds.

Here, we discuss new observations of the $\lambda 1.3$ cm (23.7 GHz) (1, 1) and (2, 2) lines of NH_3 made recently with the VLA. As is commonly understood, such observations offer the possibility of determining not only the abundance of NH_3 – thereby providing interesting insights into the diffuse gas chemistry – but the kinetic temperature T_K (Danby et al. 1988) as well. Our other observations have provided some interesting insights into the local thermal pressure (Liszt & Lucas 1998), and found it to be moderate, but the density and temperature are difficult to separate in cases of such weak excitation as occurs in diffuse clouds, even in CO. We suspect that the gas has kinetic temperatures well above those of dark clouds, both because the column densities of CO are too small to consider CO to be the main carrier of carbon and because the ratio $N(^{13}\text{CO})/N(^{12}\text{CO})$ is commonly seen to be 2–3 times higher than the isotopic abundance ratio 1:60 (Lucas & Liszt 1998), most likely due to chemical fractionation (Watson et al. 1976).

Upon finding in the new absorption data that the abundance of NH_3 was best-correlated with that of H_2CO , we reanalyzed the available data on that species, following our earlier survey

Table 1. Background sources observed in NH_3 ¹.

Source	l o	b o	$\sigma_{llc}(1, 1)$ $\times 10^{-3}$	$\sigma_{llc}(2, 2)$ $\times 10^{-3}$
B0355+508	150.3773	-1.6037	2.2	2.6
B0415+379	161.6764	-8.8186	2.0	2.2

¹ σ_{llc} = rms error in the line/continuum ratio.

(Liszt & Lucas 1995) which was published at a time when we had not yet made extensive studies of the various chemical families which are actually detectable in diffuse gas, such as OH and HCO^+ (Lucas & Liszt 1996; Liszt & Lucas 1996), CH, C_2H and C_3H_2 (Liszt & Lucas 2002; Lucas & Liszt 2000), CN, HCN and HNC (Liszt & Lucas 2001) and CS, SO, H_2 and HCS^+ (Lucas & Liszt 2002). Improved results for several sources are also available in the work of Moore & Marscher (1995). Section 2 describes our VLA and NRAO140' observations of NH_3 and discusses various elemental aspects of the molecular physics needed to interpret them. In Sect. 3 we compare the abundances of NH_3 and H_2CO with those of other species.

2. Observations and data

2.1. NH_3

2.1.1. Absorption

We observed the 23.7 GHz (1, 1) and (2, 2) lines of NH_3 at the VLA in B-configuration for three hours during the first week of 2005 March under program AL645. We used reference pointing on the background sources themselves (see Table 1). Following a bandpass calibration on J0319+415 we observed B0355+508 (NRAO150) for some 30 min, followed by almost 2 h on 3C 111 (including reference pointing). The NH_3 lines were observed simultaneously in different 128-channel IF's at spectral channel spacing 12.2 kHz or 0.154 km s^{-1} . Having foregone on-line hanning smoothing to achieve higher resolution, the actual resolution of the spectrometer is some 1.3 times lower than the channel spacing. Source characteristics and achieved rms noise levels are given in Table 1.

Reduction of the VLA data consisted of forming the bandpass cal, applying it to the sources, then forming absorption spectra using the AIPS task UVLSD. The latter is similar to UVLIN but for each integration period it uses absorption-free channels to subtract a linear spectral baseline in the uv -plane, producing an absorption spectrum, and averages all such spectra together to produce a final result. The actual flux of the background sources was not determined, but, during a 19.7 GHz observing session at the GBT in 2005 January, the fluxes were about 5 Jy and 2 Jy for B0355+508 and B0415+379, respectively. The VLA spectra achieved are shown in Figs. 1 and 2 below.

2.1.2. NH_3 emission

We earlier observed the 23.7 GHz (1, 1) and (2, 2) lines of NH_3 at the NRAO 140' during the period 1996 January 24–29.

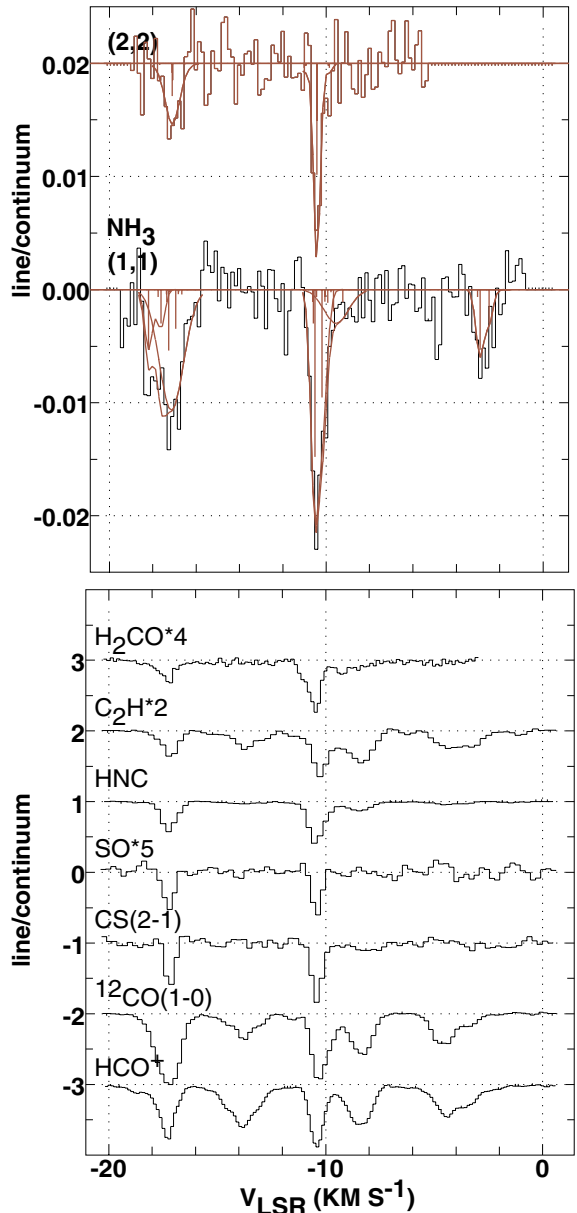


Fig. 1. Absorption spectra (line/continuum ratios) toward B0355+508 (NRAO150). *Top:* 1.3 cm (2, 2) and (1, 1) NH_3 lines and their associated Gaussian decomposition accounting for hyperfine splitting. The positions and relative intensities of individual hyperfine components are marked. *Bottom:* lines of other species, scaled as indicated.

Unfortunately, these observations, when compared to unpublished (1, 1) results of Moore and Marscher, or to the results of Nash (1990), seemed to have sizeable calibration errors (30%–40%), no doubt accruing from the relatively poor antenna performance. We do not refer to these data below for their absorption profiles, but they do suffice to place an interesting limit on the emission brightness and excitation temperature of the (1, 1) line near 3C 111, toward which strong absorption was seen in the earlier data (at $19.54 \text{ kHz} = 0.246 \text{ km s}^{-1}$ resolution). As with our earlier work on H_2CO (Liszt & Lucas 1995) at the 140', we observed off-source at positions removed by 1.2 HPBW (in this case $96''$) in each of the cardinal directions and averaged these to form an emission spectrum: the ratio of

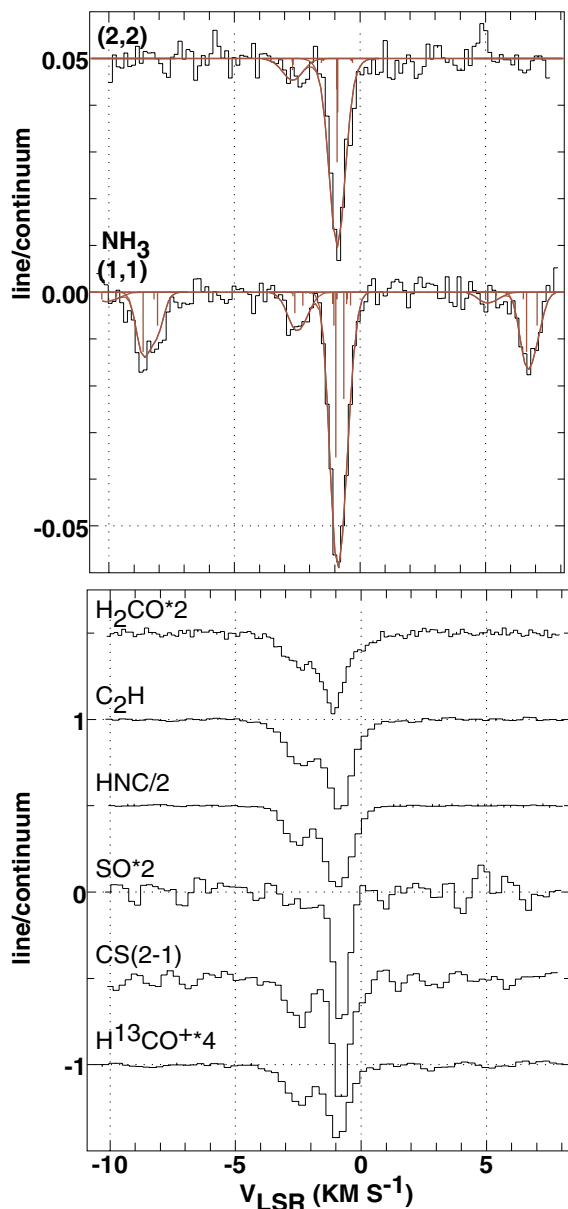


Fig. 2. As in Fig. 1, but for B0415+379 (3C 111).

emission and absorption profiles (which should be less dependent on systematic calibration errors) then implies an upper limit on the excitation given the assumptions (see Sect. 2.2.1 below).

2.2. Formulae from molecular physics

For a symmetric rotor, the rotational energies corresponding to levels (J, K) are $E(J, K)/h = BJ(J+1) + (C-B)K^2$ where, for NH_3 , the rotation constants are $B = 2.98 \times 10^{11}$ Hz ($hB/k = 14.30$ K) and $C = 1.89 \times 10^{11}$ Hz ($hC/k = 9.07$ K). Thus, $E(1, 1)/k = 23.4$ K, $E(2, 1)/k = 80.5$ K, $E(2, 2)/k = 64.9$ K and $E(3, 3)/k = 124.1$ K. Because the $K = 0$ ladder lacks half of the normal inversion levels owing to symmetry considerations, and given that it is the lower of these which is absent for $(0, 0)$, it is necessary to consider that $E(0, 0)/k = 1.1$ K corresponding to the inversion frequency of 23.7 GHz.

We assume that all the molecules are in the lowest states of the various K -ladders ($J = K$), because intraladder transitions are connected by the usual fast $\Delta J = \pm 1$ electric dipole transitions with $\mu = 1.47$ Debye. Within one (J, K) level, the inversion transitions observed here have dipole moments $\mu_{J,K}^2 = \mu^2 K^2 / J(J+1)$. The intraladder excitation temperature of the $K = 1$ ladder is shown below to be very small compared to the derived interladder rotation temperature.

All parameters mentioned here are discussed in Townes and Schawlow (1954) but the factor two degeneracy for inversion used in their formulae 46 must be replaced by $\beta = 1 + \exp(-h\nu/(kT_{\text{CMB}})) = 1.66$ since the 23.7 GHz or 1.14 K inversion splitting is not negligible compared to the excitation temperature (see the next subsection) of 2.73 K. The nuclear statistical weights of the various K ladders are 6, 3β , 3β , and 6β for $K = 0, 1, 2, 3$ respectively. The statistical weights of the various J -levels are $2J + 1$ as usual.

2.2.1. NH_3 excitation and rotation temperatures

We know from observations of other molecules (Lucas & Liszt 1996) that rotational excitation of non-metastable levels will be small. Using the single-channel (0.25 km s^{-1} resolution) rms in the average 140' emission spectrum around 3C 111, 0.0019 K, the optical depth at line center 0.022 and the nominal beam efficiency 0.4, it follows that a $2\text{-}\sigma$ upper limit on the excitation temperature within the $(1, 1)$ level is $T_{\text{EXC}}(1, 1) < 3.2$ K. Integrating over the whole line profile, one achieves a somewhat lower limit, $T_{\text{EXC}}(1, 1) < 3.0$ K. Of course, such limits on T_{EXC} are relaxed if the singledish beam is not filled, but, having detected absorption against a background point source, the intervening molecular medium cannot be too porous. We saw earlier that the excitation temperatures of CO derived in absorption and from comparison of absorption and emission are consistent with a beam-filling, largely uniform gas (Liszt & Lucas 1998). Interferometer maps of molecular emission around B0355+508, now in progress, will clarify this point.

The interladder rotational temperature between the $(1, 1)$ and $(2, 2)$ levels is found from the ratio of column densities, i.e. $T_{\text{ROT}} = -41.5 \text{ K} / \ln(3N(2, 2)/5N(1, 1))$. The relationship between T_{ROT} and the kinetic temperature T_{K} is discussed here in Sect. 3 following the calibration of the NH_3 temperature scale by Danby et al. (1988).

2.2.2. NH_3 column densities

Assuming that the excitation temperature within one (J, K) level is 2.73 K as indicated by the discussion in Sect. 2.2.1, it follows that $N(1, 1) = 3.62 \times 10^{13} \text{ cm}^{-2} \int \tau(1, 1) dv$ and $N(2, 2) = 2.71 \times 10^{13} \text{ cm}^{-2} \int \tau(2, 2) dv$ where the integrals (in units of km s^{-1}) are over all hyperfine subcomponents and the column density totals include both inversion levels. Such are tabulated in the Appendix.

Where detected (see Figs. 1 and 2), the observed absorption profiles were decomposed using a simultaneous gaussian fitting assuming LTE intensity ratios and identical linewidths for all hyperfine components within the passband. The integrated

optical depths tabulated in Tables A.1 and A.2 of the Appendix for the detected lines are sums over all hyperfine components, most but not all of which were observed and fit; the tabulated sums are extrapolated to include the others and the peak optical depth is for the strongest hyperfine component. To derive upper limits for unseen NH₃ features toward B0355+508, we first subtracted the fits corresponding to the detected features. We then calculated the rms integrated intensity over those regions of the NH₃ passband where the strongest hyperfine components of the “other” NH₃ absorption lines – those unseen but corresponding to detected HCO⁺ features – would have appeared. These limits were extrapolated to limits on the total integrated optical depth assuming LTE line ratios, then converted to column density (see also the following paragraph) and doubled to form the 2σ upper limits presented in the tables.

The total column density of NH₃ shown here was derived assuming that the ortho and para ladders are populated in proportion to their statistical weights: the column density was also calculated under the assumption that all of the rotational levels are populated at the rotational temperature determined from the (1, 1) and (2, 2) levels (perhaps by spin exchange in collisions with protons in diffuse gas, as occurs in H₂) and found to be the same within 10%. For features toward B0355+508 having only upper limits on $N(1, 1)$, we formed the ratio of total column density to $N(1, 1)$ for the detected features and applied this average value to all of the limits.

2.3. H₂CO

No new observations of H₂CO were taken for this work; rather, we blend data from our singledish survey (Liszt & Lucas 1995, their Table 1) and the contemporaneous (1994 May) VLA work of (Moore & Marscher 1995, their Table 2). We use the latter’s data for B0212, B0415, and B2200 because (being interferometer data) it is potentially better calibrated and not subject to any uncertainty induced by anomalous absorption (excitation below the cosmic microwave background which is present in the extended singledish beam and must be compensated, see Liszt & Lucas 1995). For B0355 there is good agreement between the two datasets and our work covered more kinematic components.

We relate the total column density of H₂CO to the optical depth measured at λ6 cm by assuming that the ortho:para ratio is 3:1 and that all the molecules are in the lowest J -levels of their respective (ortho and para) rotational ladders. The ortho:para ratio was actually determined to be approximately three in the work of Liszt & Lucas (1995) using a combination of cm-wave and mm-wave observations and emission was not detected at quite low levels. It follows that $N(\text{H}_2\text{CO})/T'_{\text{EXC}} = 3.68 \times 10^{13} \int \tau(1_{11} - 1_{10})dv$ using Eq. (2) in Liszt & Lucas (1995): basically one has simply that $N(\text{H}_2\text{CO})/T'_{\text{EXC}} = 1.3333 N(1_{11})/0.46$ where the factors 1.333 and 0.46 account (respectively) for the ortho/para ratio and the distribution over ortho-states when $T_{\text{EXC}} = T_{\text{CMB}}$. T'_{EXC} is the excitation temperature between the levels participating in the λ6 cm transition (1_{11} and 1_{10}), a typical value for which was found to be 1.7–2.7 K (Liszt & Lucas 1995).

Table 2. NH₃ column densities and T_{ROT} .

Source	ν km s ⁻¹	T_{rot} K	$N(\text{NH}_3)$ 10 ¹² cm ⁻²	$X(\text{NH}_3)$ ¹ 10 ⁻⁹
B0355	-17.1	17.6	2.69	4.67
	(-15, -12)		<0.53	<0.75
	-10.5	20.9	2.54	4.25
	(-9.4, -6.9)		<0.46	<0.84
B0415	(-6.9–1.5)		<0.65	<1.13
	-2.5	21.8	1.68	0.77
	-0.9	23.5	10.53	2.83

¹ Assuming $X(\text{HCO}^+) = N(\text{HCO}^+)/N(\text{H}_2) = 2 \times 10^{-9}$.

2.4. Comparison with results of Nash (1990)

Nash (1990) observed H₂CO and NH₃ toward B0355+508. As we noted previously (Liszt & Lucas 1995), her H₂CO results from the Bonn 100 m are in excellent agreement with our results from the NRAO 43 m, so that we should be able to derive NH₃ column densities from the quanta in her tables with confidence. Such derivation is mandated by the fact that she gave only upper limits on $N(\text{NH}_3)$ (despite having clearly detected several features), and the limits quoted (as multiples of 10¹⁵ cm⁻²) are suspect because they are some three orders of magnitude too generous. Most likely the table units should have been given as 10¹² cm⁻² and her limits were actually intended to have values which are slightly above the levels of our detections.

Nash (1990) very obviously detected (1, 1) absorption from the main NH₃ hyperfine components of the -17 km s⁻¹ and -10 km s⁻¹ features, and detected (2, 2) absorption from the latter. The rotational excitation temperature we derive from her results at -10 km s⁻¹ is 20.9 K, corresponding to $T_{\text{K}} \geq 24$ K, in agreement with Nash (1990) and our data (see Sect. 3.1 and Table 2): the absence of the (2, 2) feature at -17 km s⁻¹ in Nash’s data is puzzling but must remain a mystery.

3. Systematics

3.1. NH₃

Our NH₃ profiles are shown in Figs. 1 and 2 at top, where the profile decompositions are also illustrated. At bottom in each figure are shown representative profiles of other chemical families. NH₃ column densities and rotational temperatures appear in Table 2.

The rotational temperatures fall in the relatively narrow range 18–24 K and are uncorrelated with the column density, NH₃/HCO⁺ ratio, etc. According to the most recent recalibration of the NH₃ thermometer (Danby et al. 1988) the observed T_{rot} are at the upper end of the range where the kinetic temperature can reliably be inferred from observations of the (1, 1) and (2, 2) levels alone; we infer lower limits for the kinetic temperature in the range 24–30 K. For the features in which NH₃ was detected, ¹³CO is enhanced, presumably through chemical fractionation, by factors of order 3 which seems consistent with chemistry in a medium having $N(\text{C}^+)/N(\text{CO}) \gg 1$ and $T_{\text{K}} \approx 30$ K (Liszt & Lucas 1998).

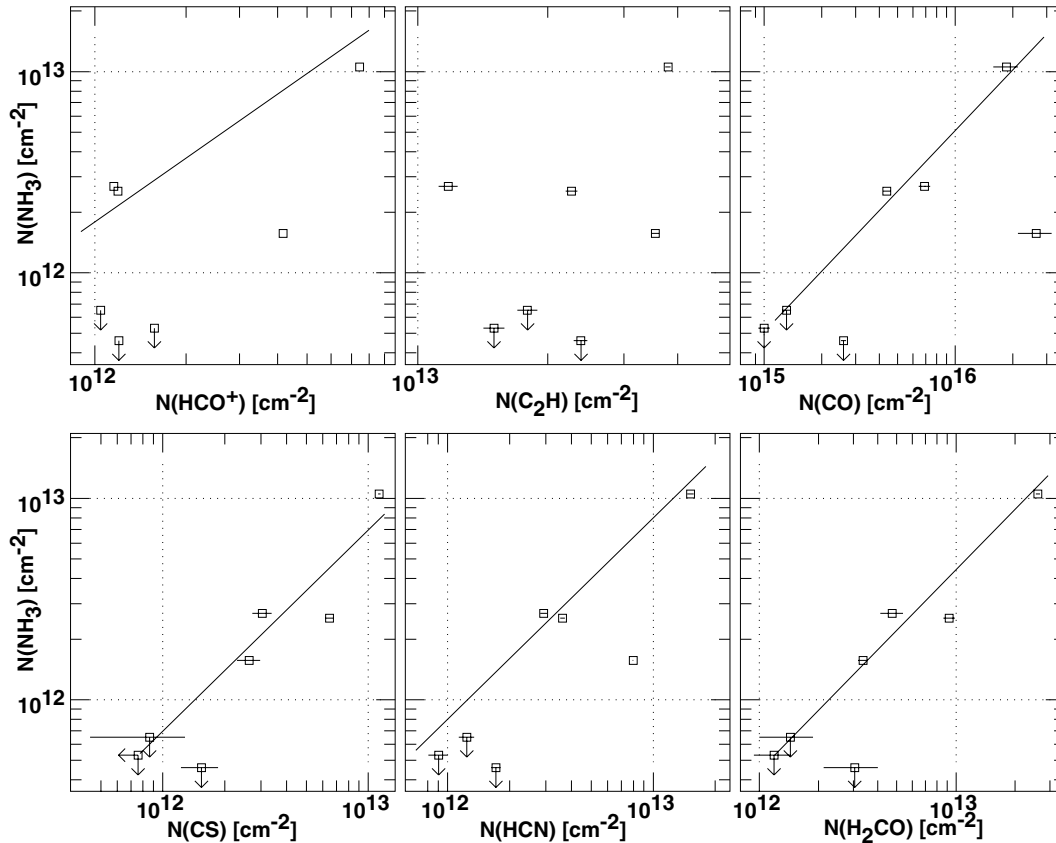


Fig. 3. Column density $N(\text{NH}_3)$ compared with those of other species found in our earlier absorption line surveys. In some cases, lines of unit slope have been superposed (these are not least-squares fits to the data). The outlying point at moderate-high column density $N(\text{HCO}^+)$, $N(\text{C}_2\text{H})$, $N(\text{CO})$ and $N(\text{HCN})$ is the cloud at -2.5 km s^{-1} toward 3C 111.

As is apparent in Figs. 1 and 2, NH_3 is one of the least frequently observed species in our sample of clouds and background sources. Its abundance ratio with respect to HCO^+ , and, therefore, most likely its abundance with respect to H_2 , $X(\text{NH}_3) = N(\text{NH}_3)/N(\text{H}_2)$, varies widely. Some aspects of the systematics are illustrated in Fig. 3 which compares column densities of NH_3 and those of other chemical families. The only reliable predictors of $N(\text{NH}_3)$ are $N(\text{CS})$ and $N(\text{H}_2\text{CO})$; the NH_3 abundance seems especially poorly-correlated with those of the hydrocarbons, represented by C_2H (see Lucas & Liszt 2000), but the range in $N(\text{C}_2\text{H})$ is somewhat limited.

3.2. H_2CO

In Liszt & Lucas (1995) we compared $N(\text{H}_2\text{CO})$ with $N(\text{HCO}^+)$ and $N(^{13}\text{CO})$, finding that H_2CO , like many species, has a rapid increase in abundance around $N(\text{HCO}^+) \approx 1 \times 10^{12} \text{ cm}^{-2}$, but not as rapid as that of ^{13}CO . We know now (Liszt & Lucas 1998) that $N(^{13}\text{CO})$ is strongly affected by fractionation, so that the H_2CO - ^{13}CO comparison, while perhaps interesting, is not directly of use in deciphering the general chemistry. In Fig. 4 we show the variation of $N(\text{H}_2\text{CO})$ with $N(\text{HCO}^+)$, $N(\text{C}_2\text{H})$, $N(\text{HCN})$ and $N(\text{CS})$. The variation of $N(\text{H}_2\text{CO})$ with $N(\text{C}_2\text{H})$ is resembles the run of $N(\text{HCN})$ with $N(\text{C}_2\text{H})$ in (Lucas & Liszt 2000) so that it is not surprising that $N(\text{H}_2\text{CO})$ and $N(\text{HCN})$ are decently correlated. H_2CO is

best correlated with $N(\text{CS})$ in Fig. 4 and it may be worth noting that the datum with the highest $N(\text{CS})$ is that for 3C 111 at -0.9 km s^{-1} , where we have preferred the $N(\text{H}_2\text{CO})$ value of Moore & Marscher (1995), which is a full factor two higher than in our own earlier work. Had we taken our own value, the correlation between CS and H_2CO would be more nearly perfect, and that between H_2CO and NH_3 in Fig. 3 somewhat less so.

4. Discussion

4.1. Overview of molecular abundances

Table 3 presents a very reductive summary of the measurements carried out in this series, updating earlier versions; the entries for “our work” in the second column are normalized to $N(\text{HCO}^+)/N(\text{H}_2) = 2 \times 10^{-9}$ and are intended to represent conditions of somewhat higher column density $N(\text{HCO}^+) \geq 10^{12} \text{ cm}^{-2}$, $N(\text{H}) \geq 10^{21} \text{ cm}^{-2}$ where the relative abundances are more stable. Species placed in the lower group in the table are rarer than those above, all of which are typically (though not invariably) found along a given line of sight. For comparison, the table also summarizes observations toward the archetypal line of sight toward $\zeta \text{ Oph}$ (from various sources as given in the footnotes there) and toward the dark cloud TMC-1 from Ohishi et al. (1992). The right-most column summarizes results from the calculations from Van Dishoeck

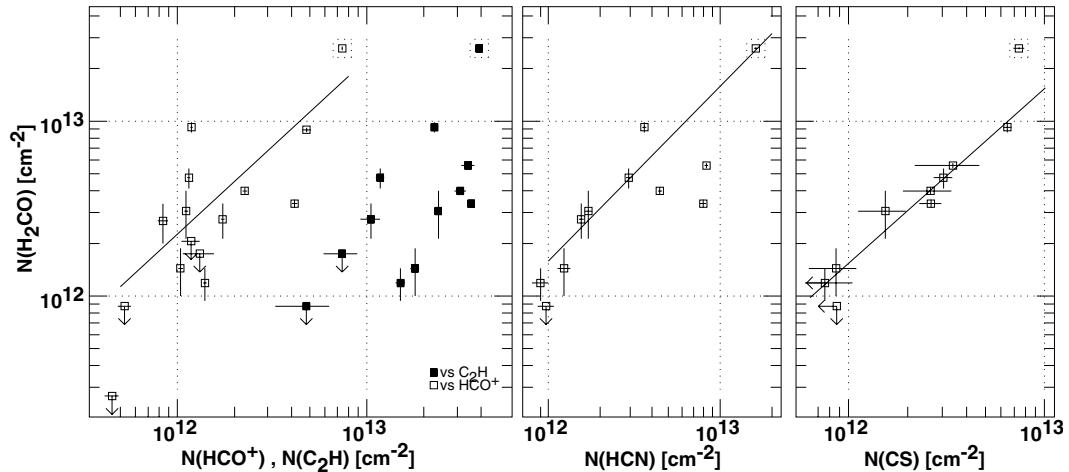


Fig. 4. Column density of H_2CO compared with those of HCO^+ , C_2H , HCN and CS. $N(\text{H}_2\text{CO})$ has been calculated assuming that the ortho:para ratio is 3 and that the excitation temperature of the $\lambda 6$ cm transition is 1.7 K. Results for the feature at -2.5 km s^{-1} toward 3C 111 are shown outlined. As in Fig. 3, lines of unit slope are shown in some cases.

Table 3. Relative abundances $10^8 \times N()/N(\text{H}_2)$.

Species	ζ Oph ¹	Our Work ²	TMC-1 ³	BD-G ⁴
OH	10	10	30	10
CO	480	300	8000	41
HCO^+		0.2-0.3	0.8	0.009
C^+	26100			89100
C	700			720
C_2	3.3			3.7
C_3	0.35			10^{-5}
CH	5.4		2	3.9
CH^+	6.3			0.006
C_2H		2.9	5-10	0.4
C_3H_2		0.14	1	
CN	0.54	2.0	3	0.30
HCN	(0.079)	0.30	2	0.007
HNC	(0.016)	0.06	2	
CS		0.25	1	
SO		0.15	0.5	
H_2CO		0.40	2	
NH	0.19			0.10
NH_3		0.20	2	

¹ Observational results for ζ Oph are as quoted by Van Dishoeck & Black (1986), except C^+ from Cardelli et al. (1993), C_3 from Maier et al. (2001), NH from Crawford & Williams (1997) and HCN and HNC are normalized to CN based on our work.

² For our work, OH and HCO^+ are discussed in Lucas & Liszt (1996) and Liszt & Lucas (1996); CO by Liszt & Lucas (1998); C_2H and C_3H_2 by Lucas & Liszt (2000); HCN, HCN and CN by Liszt & Lucas (2001); and CS and SO by Lucas & Liszt (2002).

³ Results for TMC-1 are from Ohishi et al. (1992).

⁴ BD-G is for ζ Oph model G of Van Dishoeck & Black (1986).

& Black (1986) and Van Dishoeck & Black (1988) for their model G, representing the line of sight toward ζ Oph.

The abundance of HCO^+ is somewhat lower in diffuse gas than was quoted for TMC-1. However, if abundances are measured with respect to HCO^+ , these relative abundances in diffuse gas are in most cases sensibly identical to those seen in

TMC-1. CO is the outstanding exception, typifying the dominance of C^+ in diffuse gas. Much smaller but clear exceptions are the larger CN/HCN and HCN/HNC ratios in diffuse clouds; larger HCN/HNC ratios are typical of warmer gas, as discussed in Liszt & Lucas (2001).

4.2. Summary

We presented new observations of absorption from the (1, 1) and (2, 2) levels of NH_3 toward two of the background sources studied in the previous papers in this series and our other related work. The line of sight toward B0355+508 (NRAO150) harbors some five diffuse clouds, each having an OH column density comparable to that seen toward ζ Oph ($N(\text{OH}) \approx 5 \times 10^{13}$) and NH_3 was detected from those two which show the greatest overall variety of species. The line of sight toward 3C111 has two clouds of rather higher molecular column density (3–5 \times larger $N(\text{OH})$ and $N(\text{HCO}^+)$) and NH_3 was detected from both of these, albeit only very weakly in one.

NH_3 is one of the least-commonly observed features in our sample of clouds and background sources, along with the sulfur-bearing species (CS, SO, H_2S) and H_2CO : $N(\text{NH}_3)$ and $N(\text{H}_2\text{CO})$ are quite well correlated when both species are detected. HCN is somewhat more easily detected than CS, SO, H_2CO , NH_3 , etc. but the column densities of CS and HCN, in particular, are quite well correlated. All these species tend to be found only in clouds of higher $N(\text{H}_2)$, as seen in OH and HCO^+ ($N(\text{HCO}^+) \gtrsim 10^{12}$ cm^{-2}), but the lower velocity component toward 3C 111 is deficient in NH_3 despite its high $N(\text{HCO}^+)$. Such occasional anomalies aside, when species are seen, the column density ratios among them are like those usually quoted for the dark cloud TMC-1.

The rotational temperatures found for all features with detected NH_3 fall in a rather narrow range 18–24 K, indicating an origin in cool but not very cold gas, consistent with the relatively small CO column densities and high $^{13}\text{CO}/^{12}\text{CO}$ ratios noted earlier as arising in gas where carbon is mostly in the form of C^+ .

Table A.1. Results for the (1, 1) line.

Source	ν km s ⁻¹	τ 0.001	σ_ν km s ⁻¹	$\int \tau(1, 1)d\nu$ 0.01 km s ⁻¹	$N(1,1)$ 10 ¹² cm ⁻²
B0355+508	-17.2(0.07)	5.31(0.16)	1.21(0.17)	2.94(0.06)	1.06(0.02)
	(-15, -12)			<0.54	<0.20
	-10.5(0.02)	14.80(0.50)	0.42(0.06)	2.87(0.06)	1.04(0.02)
	(-9.4, -6.9)			<0.47	<0.17
	(-6.9, -1.5)			<0.67	<0.24
B0415+379	-2.55(0.06)	4.62(0.23)	0.79(0.19)	1.68(0.06)	0.61(0.02)
	-0.91(0.08)	35.83(0.33)	0.63(0.03)	10.28(0.07)	3.72(0.03)

Table A.2. Results for the (2, 2) line.

Source	ν km s ⁻¹	τ 0.001	σ_ν km s ⁻¹	$\int \tau(2, 2)d\nu$ 0.01 km s ⁻¹	$N(2,2)$ 10 ¹¹ cm ⁻²
B0355+508	-17.1(0.08)	3.27(0.38)	0.73(0.34)	0.62(0.08)	1.68(0.27)
	-10.4(0.02)	9.34(0.36)	0.37(0.05)	0.88(0.04)	2.38(0.14)
B0415+379	-2.49(0.11)	2.74(0.35)	0.81(0.44)	0.56(0.09)	1.52(0.24)
	-0.86(0.02)	23.40(0.45)	0.65(0.05)	3.90(0.08)	10.57(0.22)

Finding that $N(\text{NH}_3)$ was best correlated with $N(\text{H}_2\text{CO})$ we analyzed available measurements of the latter in diffuse clouds. The column density of H_2CO is well-correlated with $N(\text{CS})$ as well and where detected – in a much larger survey than has been performed for NH_3 – the ratio $N(\text{H}_2\text{CO})/N(\text{HCO}^+)$ takes on values typical of TMC-1.

The origin of NH_3 in dense dark gas is now understood as arising in the gas phase through pathways originating with either N^+ or N , while H_2CO is presumed to be formed on dust. Why these species should be so well correlated with each other in diffuse clouds, and why they ever appear there with such high abundances is an ongoing mystery.

4.3. Future work

Detecting unexpectedly high abundances of complex molecules along lines of sight lacking dark gas has raised many unanswered questions about interstellar chemistry and the structure of the diffuse interstellar medium. In the next and probably final paper in this series we will discuss line of sight properties and statistics based on an extensive new survey of atoms, molecules and extinction along the lowest-latitude (and hence longest) lines of sight available for study at the present time.

Acknowledgements. The National Radio Astronomy Observatory is operated by AUI, Inc. under a cooperative agreement with the US National Science Foundation. IRAM is operated by CNRS (France), the MPG (Germany) and the IGN (Spain). We owe the staff at IRAM (Grenoble) and the Plateau de Bure our thanks for their assistance in taking the data. We thank the referee for an especially close reading of the text. This paper is dedicated to the memory of Ana Nash.

Appendix A: Products of Gaussian fitting and profile integrals

References

- Boland, W., & de Jong, T. 1982, ApJ, 261, 110
 Cardelli, J. A., Mathis, J. S., Ebbets, D. C., & Savage, B. D. 1993, ApJ, 402, L17
 Chieze, J. P., & Pineau Des Forets, G. 1989, A&A, 221, 89
 Chieze, J.-P., Pineau des Forets, G., & Herbst, E. 1991, ApJ, 373, 110
 Cox, P., Güsten, R., & Henkel, C. 1988, A&A, 206, 108
 Crawford, I. A., & Williams, D. A. 1997, MNRAS, 291, L53
 Danby, G., Flower, D. R., Valiron, P., Schilke, P., & Walmsley, C. M. 1988, MNRAS, 235, 229
 Federman, S. R., & Allen, M. 1991, ApJ, 375, 157
 Le Bourlot, J. 1991, A&A, 242, 235
 Liszt, H., & Lucas, R. 2001, A&A, 370, 576
 Liszt, H., & Lucas, R. 2002, A&A, 999, 888
 Liszt, H. S., & Lucas, R. 1995, A&A, 299, 847
 Liszt, H. S., & Lucas, R. 1996, A&A, 314, 917
 Liszt, H. S., & Lucas, R. 1998, A&A, 339, 561
 Lucas, R., & Liszt, H. 1998, A&A, 337, 246
 Lucas, R., & Liszt, H. S. 1996, A&A, 307, 237
 Lucas, R., & Liszt, H. S. 2000, A&A, 358, 1069
 Lucas, R., & Liszt, H. S. 2002, A&A, 384, 1054
 Maier, J. P., Lakin, N. M., Walker, G. A. H., & Bohlender, D. A. 2001, ApJ, 553, 267
 Moore, E. M., & Marscher, A. P. 1995, ApJ, 452, 671
 Nash, A. G. 1990, ApJS, 72, 303
 Ohishi, M., Irvine, W., & Kaifu, N. 1992, in Astrochemistry of cosmic phenomena: Proc. of the 150th Symposium of the International Astronomical Union, held at Campos do Jordao, Sao Paulo, Brazil, August 5–9, 1991, ed. P. D. Singh (Dordrecht: Kluwer), 171
 Scott, G. B. I., Freeman, C. G., & McEwan, M. J. 1997, MNRAS, 290, 636
 Van Dishoeck, E. F., & Black, J. H. 1986, ApJS, 62, 109
 Van Dishoeck, E. F., & Black, J. H. 1988, ApJ, 334, 771
 Watson, W. D., Anicich, V. G., & Huntress, W. T. J. 1976, ApJ, 205, L165
 Xie, T., Allen, M., & Langer, W. D. 1995, ApJ, 440, 674